View metadata, citation and similar papers at core.ac.uk
brought to you by CORE
provided by Eldorado - Ressourcen aus und für Lehre, Studium und Forschung

Effect of Conductivity of the Inner Rod on the Collision Conditions During a Magnetic Pulse Welding Process

T. Sapanathan[1*], K. Yang[1], R. N. Raoelison[1, 2], N. Buiron[1], D. Jouaffre[3], M. Rachik[1]

[1] Sorbonne universités, Université de Technologie de Compiègne, Laboratoire Roberval, CNRS UMR 7337, Centre de Recherche Royallieu, CS 60319, 60203 Compiègne cedex, France
[2] Université de Bourgogne Franche Comté, IRTES-LERMPS, Université de Technologie de Belfort Montbéliard, 90100 Belfort, France
[3] PFT INNOVALTECH, 02100 Saint-Quentin, France
[*]Corresponding author. Email: thaneshan.sapanathan@utc.fr

Abstract

The Magnetic Pulse Welding (MPW) process involves a high speed collision between the flyer and inner rod. Conductivity of the inner rod may play a significant role in the collision speed and collision angle. The collision conditions were investigated with varying conductivity of the inner rod in this study. Coupled mechanical-electromagnetic 3D simulations were carried out using LS-DYNA package to investigate the effect of conductivity of the inner rod on the collision patterns during the MPW process. The simulation involves a welding process with a tube and a rod using a one turn coil with a separate field shaper. The electrical conductivity was varied to a wide range to investigate the influence on the collision condition. Moreover, in order to verify the independency of the collision condition with the mechanical properties of the inner rod, two cases including aluminum alloy AA2024-T351 and copper with appropriate Johnson-Cook parameters were used for the rod. In the entire simulations aluminum alloy was used as the tube material. It was identified that the impact velocity is almost consistent for each case and the impact angles vary between negative and positive values according to the angular measurement convention used in this study. Although, influence of the conductivity of the inner rod is not significant for the investigated current flow while it may sometime delay the incidence of collision at lower frequencies than the critical frequency (F_{Crit}). Optimizing the collision conditions in the MPW process can help to identify the suitable materials for prescribed welding conditions.

Keywords

Magnetic pulse welding, Numerical modelling, Collision velocity

1 Introduction

Interface characterization is used to ensure the weldability of the materials in various joining applications. The wavy interface produced during the collision is a unique feature of the impact welding that was also experimentally evidenced to identify potentially permanent weld while defective joints appear with the degradation and highly deformed interfaces (Baaten et al., 2010). In the literature, the notion of weldability is described and experimentally confirmed depending on the development of interfacial waves and the research works on this subject result in the identification of suitable parameters for weld creation. Early studies revealed that jetting and hydrodynamic conditions at the interface govern the weldability windows for impact welding processes. Suitable conditions for weld formation were also theoretically established using a correlation between collision angle and impact velocity which served as a reference for further development to describe the welding range.

The welding range may consist of several different zones, viz., pre-critical zone (no welding), wavy zone (welding zone) and unfavorable zone including waveless zone, anomalous wave zone, melt solidification zone and supersonic zone (Lysak and Kuzmin, 2012). But waveless interface without apparent deformation, wavy morphology and interface deterioration are practically evidenced at the interface and they allow a pragmatic distinction of a successful welding range (Raoelison et al., 2013, Nassiri et al., 2015). In accordance with the aforementioned reason, the weldability in impact welding is currently related to the morphology of the interface and particularly with the wavy shape. Moreover, the major criteria of bonding used in an impact welding remains the transition from smooth to wavy morphology.

Although, formation of wavy interface and its characteristics such as high amplitude and large wavelength are considered as an indication of a strong bonding (Zamani and Liaghat, 2012, Xu et al., 2013), recent research studies reported that these parameters may not be crucial for the formation of bonding. In contrast, jetting and ejection of materials from the interface are identified as required phenomena to create a successful bonding, which mainly depend on the collision conditions such as collision speed and collision angle (Groche and Pabst, 2015). These ejected materials may consist of oxides or solid parent materials (Kakizaki et al., 2011, Pabst and Groche, 2014) that may also include burnt properties which depend on the temperature of the interface (Pabst and Groche, 2014). Negative or zero degree collision angles may hinder the weld formation and that could weaken the welding due to the accumulation of the ejected materials at the interface. At the same time, very high impact velocity (i.e. higher than the speed of sound in the material), the jetting phenomenon becomes impossible because the gap closure speed is higher than

that of the jet, which traps the ejected material in place (Lysak and Kuzmin, 2012, Groche and Pabst, 2015). Therefore it is important to determine the collision conditions at the interface to obtain the favorable welding conditions.

During a magnetic pulse welding the conductivity of individual parts and the conductivity difference between the welding components can influence the impact conditions and the associated ejection phenomena during the weld formation by influencing the collision speed and the collision angle. This could be a main difference between MPW and other impact welding processes. This study presents an investigation on the effect of the conductivity of the inner rod during a weld formation in a magnetic pulse welding process for materials with various electromagnetic properties.

2 Methods

Coupled electromagnetic-mechanical simulations with 3D models (**Fig. 1a**) are used to investigate the welding conditions in terms of collision speed and collision angle while varying the conductivity of the inner rod. The input current obtained for the coil using a Rogowski probe for 8 kV input voltage from a custom made generator is used in the simulation. The current curve and specifications of the main working area are respectively given in **Fig. 1b** and **1c.**

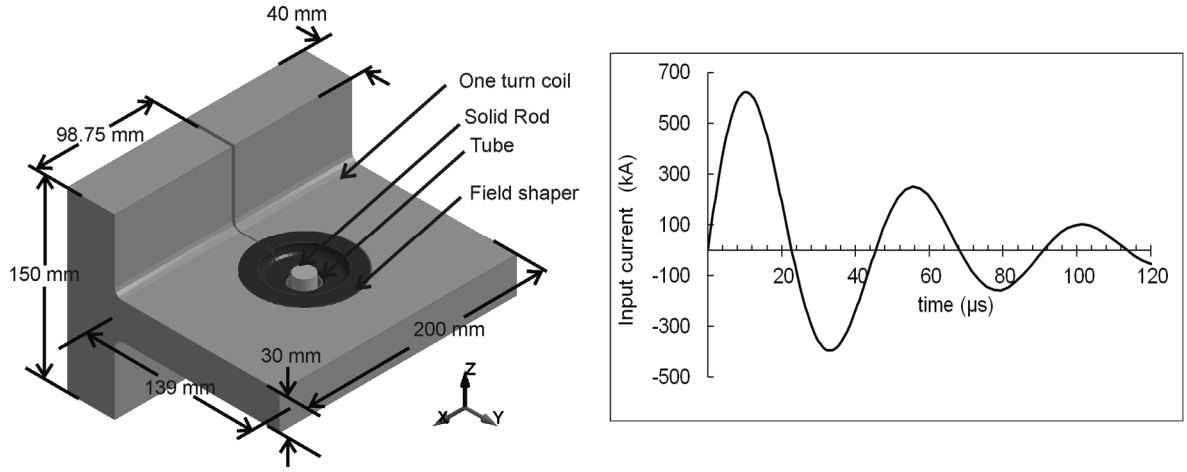

(a) (b)

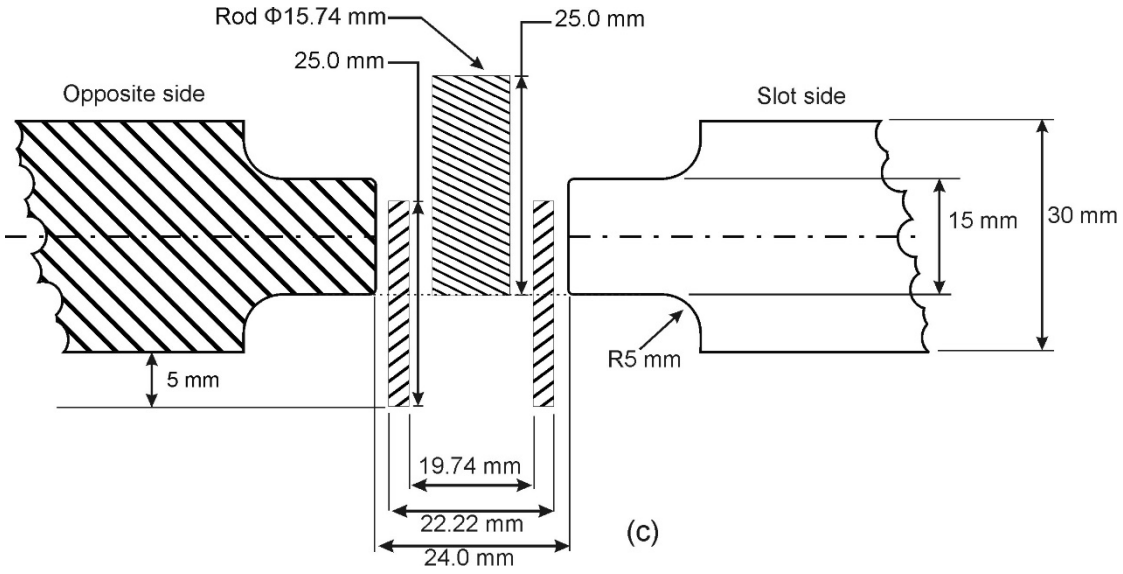

***Figure 1**: 3D model (a) and the input current (b) used in the numerical simulations, and the schematic illustration of the test case (c).*

Mechanical and electromagnetic properties used for each component in the welding assembly are given in **Table 1**. Material behavior of the deformable parts under high strain rate was defined in the simulations using Johnson-Cook material model (Eq. 1) and the corresponding parameters obtained from literatures for aluminum (Mabrouki et al., 2008) and copper (Johnson and Cook, 1985) are provided in **Table 2.**

Material	Components	Density ($kg.m^{-3}$)	Young's modulus (GPa)	Poisson's ratio	Electrical conductivity (IACS%)
AA2024 – T351	Tube or Rod	2700	73	0.33	5%, 30%, 60%, 90%
Commercially pure copper	Tube or Rod	8900	124	0.34	5%, 30%, 60%, 90%
Copper Alloy	Field shaper	7900	210	0.29	46%
Steel	Coil	Rigid			7%

***Table 1**: Mechanical and electromagnetic properties of components and their materials used in this model, where 100% IACS is equivalent of 5.8001 × 10^7 $S.m^{-1}$.*

Johnson-Cook parameters	*A* (MPa)	*B* (MPa)	*C*	*n*
Aluminum alloy AA2024-T351	352	440	0.0083	0.42
Commercially pure copper	90	292	0.025	0.31

***Table 2**: Johnson-Cook parameters used for the constitutive behavior of aluminum alloy AA2024-T351 and commercially pure copper during the simulations.*

$$\bar{\sigma} = (A + B\bar{\varepsilon}^n)\left[1 + Cln\left(\frac{\dot{\bar{\varepsilon}}}{\dot{\bar{\varepsilon}}_0}\right)\right] \quad (1)$$

The following 9 cases (**Table 3**) were investigated in the simulation for impact velocity and the collision angle at the onset of impact. Although, the simulation did not include the microscopic interfacial effect to capture the welding effect, these models are sufficient to obtain the impact conditions. Automatic surface to surface contact was prescribed between workpieces to capture the contact behavior during the collision. The collision angles were calculated based on the angle between the velocities component (V_r and V_z) from the simulations. The sign conventions used in the angle and velocity predictions are provided in **Fig. 2**. A high magnification view near the top edge of the tube shown in **Fig. 2b** represents the possible in-flight kinematics of the flyer tube.

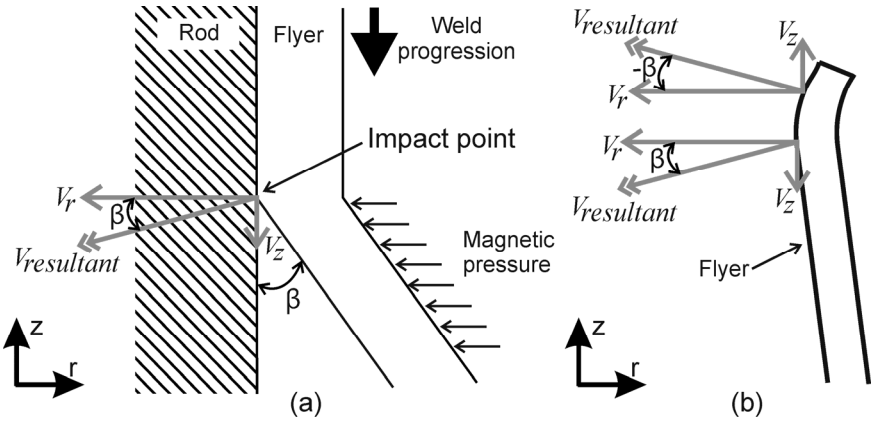

***Figure 2**: (a) Sign convention used for velocity and angle predictions in this study and (b) a detailed view of the positive and negative angles near the top edge of the flyer.*

The simulations were carried out using LS-DYNA® package with the solver version R8. The electromagnetic-mechanical multi-physics solver uses both finite element method (FEM) and boundary element method (BEM) (Çaldichoury and L'Eplattenier, 2012). These simulations provide an ideal condition to investigate the conductivity effect on the collision conditions, where the representations of materials are not 100 percent accurate with the reality. However, conductivity values are carefully chosen within the reality of conductivity limits (5% - 90 % IACS) in this study.

Moreover, solution time steps are important input parameters that govern the convergence of a simulation. In an electromagnetic-mechanical coupling, that requires for both electromagnetic and mechanical time steps for a simulation. In general, the electromagnetic time step, $\Delta T \leq p^2/2D$, where p and D are characteristic mesh size and characteristic diffusion time. The characteristic diffusion time D is determined by, $D = 1/\mu\sigma$, where μ and σ respectively denote magnetic permeability and electric conductivity of the conductor. The mechanical time step (Δt) is always smaller than the electromagnetic time step, $\Delta t \ll \Delta T$.

	Case 1	Case 2	Case 3	Case 4	Case 5	Case 6	Case 7	Case 8	Case 9
Tube material and conductivity	Al, 30%	Al, 30%	Al, 30%	Al, 30%	Al, 30%	Al, 30%	Al, 30%	Al, 30%	Cu, 30%
Rod material and conductivity	Al, 5%	Al, 30%	Al, 60%	Al, 90%	Cu, 5%	Cu, 30%	Cu, 60%	Cu, 90%	Cu, 30%

***Table 3**: Mechanical behavior of material and electromagnetic properties considered for the corresponding material in various simulation cases.*

3 Results and Discussion

Although, validation procedure for the numerical model is still in progress, the preliminary observations of the overall final shape for a welded sample obtained under similar experimental setting **(Fig. 3b)** corroborate the predicted final deformed shape of the samples (**Fig. 3a)**. Further measurements and interfacial observations for the particular case are required to validate the numerical model. Sample shown in Fig. 3b, is obtained from a pool of previous experiments and details of welded samples obtained under various parameters with their weld variances could be found elsewhere (Raoelison et al., 2015). Mechanical strength of those welds were characterised using push-out and torsion-shear tests (Raoelison et al., 2013).

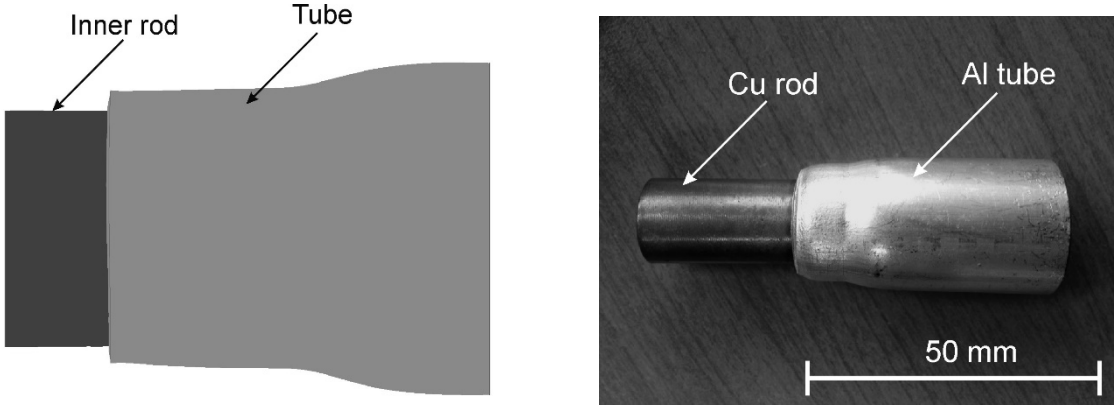

***Figure 3**: Final shape of the welded specimen from numerical simulations in comparison with MPW sample; (a) weld region of the numerical model at the end of the simulation (b) magnetic pulse welded Al/Cu sample*

The impact velocity was calculated inside of the tube along the longitudinal direction. Sudden change of velocity was used to identify the onset of the impact velocity. Immediately at the onset of the impact, the resultant velocity of the tube rapidly reduces. Based on the calculation of the resultant velocity, and angle of attack [tan^{-1} *(Vz/ Vr)*] were calculated for the corresponding onset time.

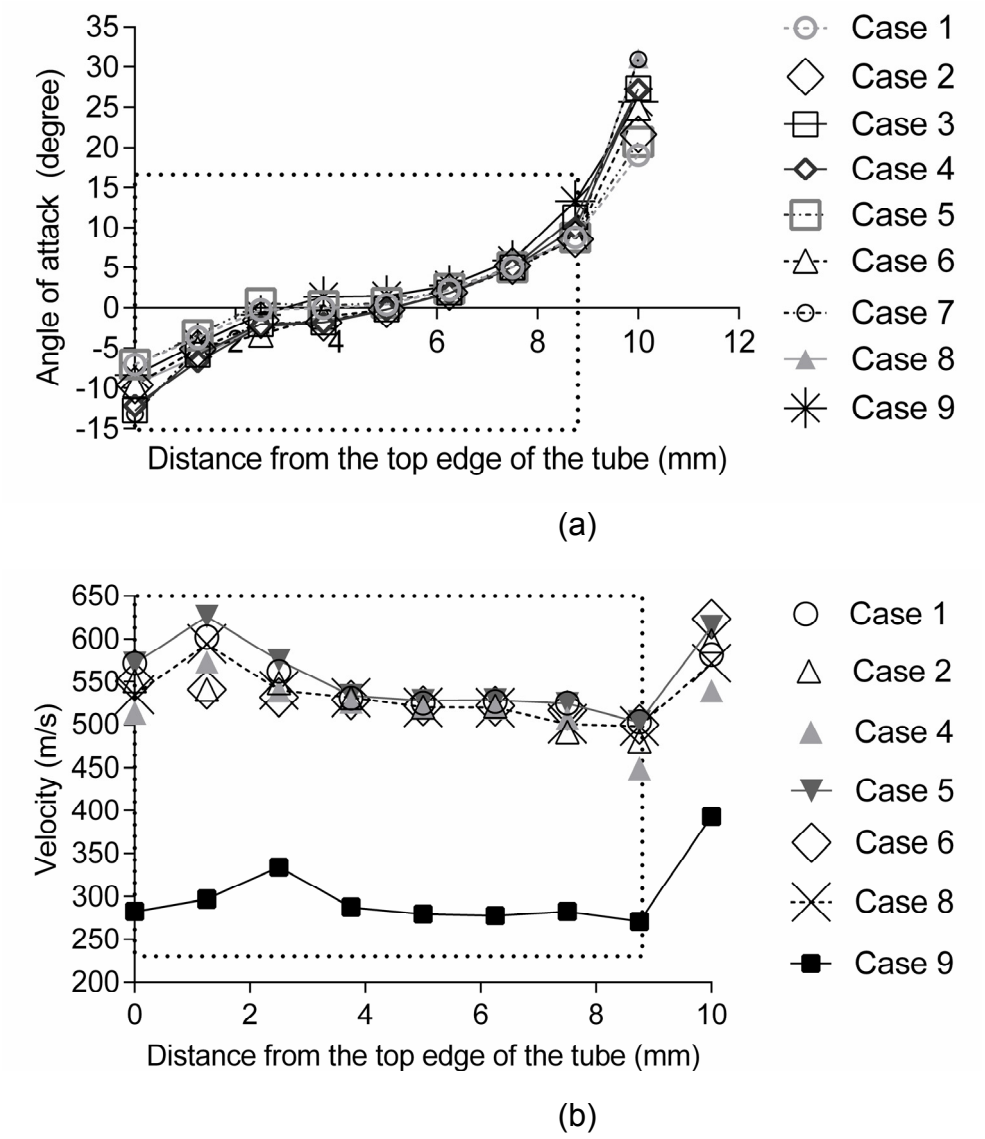

***Figure 4**: Impact angles along the longitudinal distance from the top edge of the tube for the simulation cases of 1 to 9 in (a) and instantaneous resultant velocity at those corresponding points during the onset time of the impact in (b). The boxed regions in (a) and (b) well represent the onset of impact.*

The impact velocity is plotted against the longitudinal distance from the top edge of the tube (**Fig. 4b**) and results indicate almost consistent throughout the entire weld length (~0 - 9 mm). Impact angle measured with the radial direction and positive sign convention used for the anti clockwise impact angles. Impact angles obtained along the longitudinal directions corresponding to those impact velocity points in Fig. 4b, shown in **Fig. 4a**. The impact angles vary between positive and negative in the impact region according to the sign convention (Fig. 2) used in this study. Outside of the boxed regions in Fig 4a and 4b do not represent the impact because the tube was not able to come in contact with the rod in those

outside regions. It's also in agreement with the experimental case where ~9 mm tube length was in contact with the rod (Fig. 3b).

There are almost very similar behaviors observed for the same electrical conductivity cases, regardless of the parts' mechanical parameters. That is, pairs of (Case 1 and Case 5), (Case 2 and Case 6), (Case 3 and Case 7) and (Case 4 and Case 8) show a close agreement in comparison with other results. However, the variations were not significant in these case studies. A control case was considered with the mechanical properties of copper tube (Case 9), impact angles obtained from this case deviate from other cases of 1-8. Moreover the velocity was consistent for all the cases of 1-8 and that significantly differs from the Case 9 as expected.

Although these case studies indicate that the influence of the conductivity of the inner rod on the impact angle and impact velocity is not apparent, the influence was identified as highly depended on the current frequency. That is, one could neglect the conductivity of the inner rod when considering various materials for welding at higher frequencies than that of a critical frequency (F_{Crit}) that can be obtained by equating the onset of collision time and the diffusion time for the magnetic field to reach the inner surface from the outer, through thickness direction of the flyer tube. At those higher frequencies ($>F_{Crit}$) the impact occurs before the full diffusion of magnetic field through thickness from the exterior to the inner surface of the tube while at lower frequencies ($<F_{Crit}$) impact may occur after the full diffusion of magnetic field through thickness of the tube, hence those events fully depend on the individual input current frequency.

Therefore, this study was further extended to investigate diffusion time and magnetic field at various locations. The magnetic field is parallel to the axis of tube and it diffuses through thickness from the outer surface of the tube. Magnetic field in the tube can be calculated for a particular position along the z axis using Eq. 2 in a cylindrical coordinate system.

$$B(t,d) = b\exp\left(-\alpha t - \frac{d}{\delta}\right)\sin(\omega t - \frac{d}{\delta}) \tag{2}$$

where t, d, δ, b, α and ω are respectively time and distance from the external surface, skin depth, amplitude factor, time damping constant and angular frequency. Constants b, α and ω are decided by the source current. In this equation, the terms "$exp\ (-\alpha t - d/\delta)$" and "$sin\ (\omega t - d/\delta)$" respectively denote the damping and periodic components. The magnetic field diffusion reaches a particular point when "$(\omega t - d/\delta=0)$". Based on these aforementioned equations, the diffusion time for the inner surface of the tube (when $d=1.24$ mm, equivalent to the thickness of the tube and the electrical conductivity of 30 IACS% for all the cases) can be estimated as ~10.7 µs. This diffusion time to the inner surface is identified as just 1 µs before impact time. However, the full diffusion of the current requires extra time; the influence of the initial diffusion within the 1 µs is negligible.

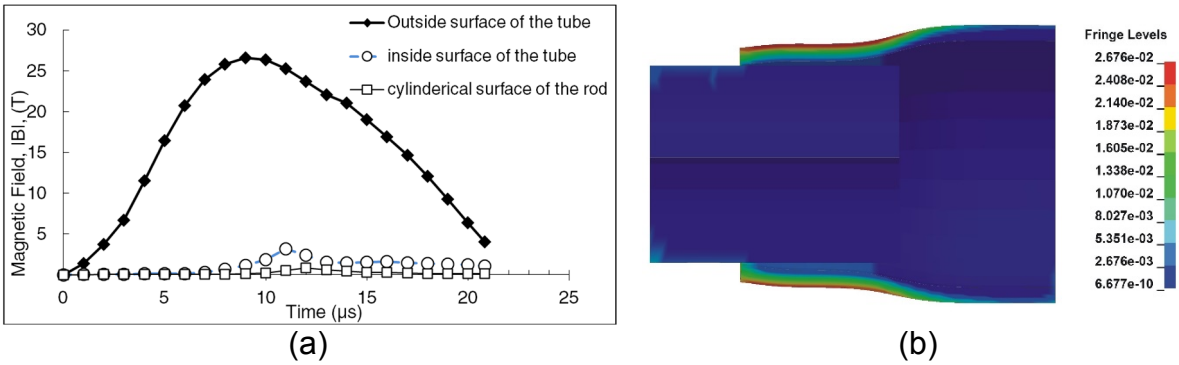

***Figure 5**: Magnetic field strength obtained for the Case 2 along the mid plane of the field shaper at various locations against time in (a) and magnetic flux density in kilo Tesla obtained along the longitudinal section at 11 µs in (b).*

Magnetic field strength at the locations of the outer surface of the tube, inner surface of the tube and the cylindrical surface of the rod against time for the first half period of the input current are shown in **Fig. 5a**. These results clearly indicate the shielding effect of the tube during the diffusion time that blocks almost 100% of the magnetic field reaching inside the tube. **Fig. 5b** explains the magnetic field diffusion through thickness just after the diffusion reaches the inner surface of the tube at 11 µs.

4. Conclusions

This study was carried out to investigate the influence of the conductivity of inner rod on the collision velocity and collision angle during a magnetic pulse welding process. The simulations were performed under the same process conditions with varying material properties. The impact velocities were captured at the onset of the collision and the impact angles were determined from the direction of the velocity at the onset. It was identified that the impact velocity is almost consistent for each case within the contact region, while the impact angles vary between negative and positive values according to the angular measurement convention used in this study. This study also clearly shows that the impact velocity changes from a positive z with r coordinate to negative z with r coordinate during the welding process. However, the influence of the conductivity of the inner rod on the impact angle and impact velocity are not well captured within the resolution of the data points, and which is identified as highly influenced by the diffusion time and the magnetic field strength at the inner surface of the flyer tube before the onset of the collision. Moreover, this study reveals at high current frequencies, higher than the critical frequency (F_{Crit}), one can neglect the effect of conductivity of the inner rod during a magnetic pulse welding process.

Acknowledgments

Authors would like to acknowledge the "Région Picardie" and "Le fonds européen de développement régional (FEDER)" for their financial support and "Plateforme Innovaltech" for its collaboration.

References

Baaten, T., N. Debroux, W. De Waele and K. Faes, 2010. Joining of copper to brass using magnetic pulse welding. 4th International Conference on High Speed Forming, Dortmund.

Çaldichoury, I. and P. L'Eplattenier, 2012. EM Theory Manual. Electromagnetism and Linear Algebra in LS-DYNA, Livemore Software Technology Corporation.

Groche, P. and C. Pabst, 2015. Numerical simulation of impact welding processes with LS-DYNA. 10th European LS-DYNA Conference, Würzburg, Germany.

Johnson, G. R. and W. H. Cook, 1985. *Fracture characteristics of three metals subjected to various strains, strain rates, temperatures and pressures*. Engineering fracture mechanics 21(1), pp. 31-48.

Kakizaki, S., M. Watanabe and S. Kumai, 2011. *Simulation and experimental analysis of metal jet emission and weld interface morphology in impact welding*. Materials transactions 52(5), pp. 1003-1008.

Lysak, V. and S. Kuzmin, 2012. *Lower boundary in metal explosive welding. Evolution of ideas*. Journal of Materials Processing Technology 212(1), pp. 150-156.

Mabrouki, T., F. Girardin, M. Asad and J.-F. Rigal, 2008. *Numerical and experimental study of dry cutting for an aeronautic aluminium alloy (A2024-T351)*. International Journal of Machine Tools and Manufacture 48(11), pp. 1187-1197.

Nassiri, A., G. Chini, A. Vivek, G. Daehn and B. Kinsey, 2015. *Arbitrary Lagrangian–Eulerian finite element simulation and experimental investigation of wavy interfacial morphology during high velocity impact welding*. Materials & Design 88, pp. 345-358.

Pabst, C. and P. Groche, 2014. Electromagnetic Pulse Welding: Process Insights by High Speed Imaging and Numerical Simulation. 6th International Conference on High Speed Forming, South Korea.

Raoelison, R., N. Buiron, M. Rachik, D. Haye, G. Franz and M. Habak, 2013. *Study of the elaboration of a practical weldability window in magnetic pulse welding*. Journal of Materials Processing Technology 213(8), pp. 1348-1354.

Raoelison, R. N., T. Sapanathan, N. Buiron and M. Rachik, 2015. *Magnetic pulse welding of Al/Al and Al/Cu metal pairs: Consequences of the dissimilar combination on the interfacial behavior during the welding process*. Journal of Manufacturing Processes 20, Part 1, pp. 112-127.

Xu, Z., J. Cui, H. Yu and C. Li, 2013. *Research on the impact velocity of magnetic impulse welding of pipe fitting*. Materials & Design 49, pp. 736-745.

Zamani, E. and G. H. Liaghat, 2012. *Explosive welding of stainless steel–carbon steel coaxial pipes*. Journal of Materials Science 47(2), pp. 685-695.